GRAPH THEORY AND THE ANALYSIS OF FRACTURE NETWORKS

David J. Sanderson[1]*, David C.P. Peacock[2], Casey W. Nixon[2], Atle Rotevatn[2]

[1] Ocean and Earth Science, University of Southampton, National Oceanography Centre, Southampton SO14 3ZH, UK

[2] Department of Earth Science, University of Bergen, P.O. Box 7800, 5020 Bergen, Norway.

* Corresponding author email: d.j.sanderson@soton.ac.uk

Abstract

Two-dimensional exposures of fracture networks can be represented as large planar graphs that comprise a series of branches (B) representing the fracture traces and nodes (N) representing their terminations and linkages. The nodes and branches may link to form connected components (K), which may contain fracture-bounded regions (R) or blocks. The proportions of node types provide a basis for characterizing the topology of the network. The average degree <d> relates the number of branches (|B|) and nodes (|N|) and Euler's formula establishes a link between all four elements of the graph with |N| - |B| + |R| - |K| = 0.

Treating a set of fractures as a graph returns the focus of description to the underlying relationships between the fractures and, hence, to the network rather that its constitutive elements. Graph theory provides a wide range of applicable theorems and well-tested algorithms that can be used in the analysis of fault and fracture systems. We discuss a range of applications to two-dimensional fracture and fault networks, and briefly discuss application to three-dimensions.

Key words:

Fracture networks; graph theory; topology

Highlights:

- Fracture networks considered as large planar graphs, consisting of nodes, branches, regions and components.
- Evaluation of metrics to describe fracture networks
- Future developments in fracture network characterization

1. Introduction to fracture networks

In his famous treatise on mineral mining, Georgius Agricola (1558) showed that veins form networks. His amazing woodcuts (Fig. 1a) show these vein networks as they intersect the surface and also his three-dimensional interpretation in the sub-surface. He proposed that veins both bifurcate and cross-cut one another (Fig. 1b), noting their relative position and inferred age rather than presenting details of their size and orientation. His was very much a topological view of fracturing, dating from some 180 years before Leonhard Euler's (1736) work that laid the foundations of graph theory and topology.

In mathematics, a ***graph*** is a structure comprising a set of ***nodes*** (or vertices), with pairs of nodes linked by ***branches*** (or edges). Using this definition, we can represent a fracture network as a graph, whereby the fractures are the branches and the nodes are their tips and intersections (Fig. 1c). Graph theory examines the relationships between the nodes and branches that are independent of their geometry (e.g. position, length, orientation), and hence it can be used to describe the topology of a fracture network (e.g., Jing and Stephansson, 1994; 1997). We use 'graph' in this quite specific sense throughout the paper, and it should not be confused with other uses, such as for charts or sketching of functions. Graphs have a wide range of applications in other fields (Table 1) and many useful analogies exist when considering fracture networks. Here, we focus on some basic ideas, mainly in two-dimensions, and then suggest some areas for future development. For details and formal proofs of the basic theorems, the reader is referred to standard works on network topology and graph theory (e.g., West, 1996; Wilson, 1996; Bondy and Murty, 2008).

In the last 450 years, and particularly in the 20th Century, there has been a progressive advance in understanding of: a) fracture geometries, with millions of fracture orientations being plotted on stereograms and rose diagrams; b) kinematics of fracture opening and shear; and eventually c) the application of fracture mechanics (e.g. Pollard and Aydin, 1988). Yet there has been little application of topology and graph theory to understanding the relationships between fractures and their interactions, although Hancock (1985) did propose a system of using capital letters in the Latin alphabet to describe the style of a joint system that has parallels with the nodal system described below.

By going back to examining the relationship between fractures, as Agricola (1558), we outline a new approach to fracture networks using graph theory, which allows us to move beyond simple description of geometric parameters (e.g. orientation and length). In this paper, we will explore how some basic ideas of graph theory, mainly in two-dimensions, contribute to an understanding of how fractures in a network are related, distributed and inter-connected. This approach shifts emphasis

63 to the network as a whole rather than focussing only on the components, and provides new insights
64 into fracture-related processes, e.g. fluid flow models.

65 2. Networks, topology and graphs

66 A fracture network is a system of fractures developed within a rock volume (Fig. 1d), where the
67 positions, orientations and relationships between the individual fractures are mapped in two- or
68 three-dimensions. The fractures may or may not intersect. Where they do so, they form intersection
69 lines in three-dimensions that appear as points or nodes where they cut a two-dimensional surface.
70 The fractures that develop in a single deformation event are likely to have interrelated kinematics
71 and mechanics. Fractures may be active during different events, including earlier formed fractures
72 commonly being reactivated during later events. Understanding fracture networks requires both an
73 analysis of the individual fractures and of networks as a whole.

74 2.1 Node/branch model

75 The node/branch model (Manzocchi, 2001; Sanderson and Nixon, 2015) divides a fracture trace into
76 a series of ***branches*** (B), each with a ***node*** (N) at both ends (Fig. 1c). The branches may represent
77 fractures of any type (opening mode fractures, faults, deformation bands, stylolites, etc.). The nodes
78 represent the tips and intersections of fractures and are important because they indicate locations
79 where a fracture interacts with the rock or another fracture. This representation scheme can be
80 applied at all scales, from micro-fractures within grains to tectonic plates (Fig. 2a).

81 Three types of node are commonly found in two-dimensional fracture networks: I-nodes at the
82 isolated tips of fractures; Y-nodes where one fracture meets or abuts against another; and X-nodes
83 where two fractures cross-cut one-another. To understand why two-dimensional exposures of
84 fracture networks are dominated by these three node types, we need to realise that they are
85 branch-generated rather than node-generated. By this we mean that the fractures represent the
86 fundamental physical element, with the nodes describing how the fractures relate to one another. If
87 the fractures remain isolated, their tips are I-nodes. If two fractures abut, we get Y-nodes, whereas if
88 the fractures cross-cut one another, we get X-nodes. The possibility of a system of fractures
89 intersecting or crossing at nodes with more than four branches is negligible, which contrasts with
90 many social and communication networks where people or locations (nodes) may have friendships
91 and other interactions represented by any number of branches.

92 An initial step in characterising a fracture network is to count the number of nodes (|N|) of each
93 type - |I|, |Y| and |X|.

94 $$|N| = |I| + |Y| + |X| \quad (1)$$

Since an I-node has 1 branch, a Y-node has 3 branches and an X-node has 4 branches, and each branch has a node at each end, if follows that the number of branches |B| is:

$$|B| = (|I| + 3|Y| + 4|X|)/2 \quad (2)$$

The proportion of each node type (P) is:

$$P_I = |I|/|N|,\ P_Y = |Y|/|N| \text{ and } P_X = |X|/|N| \quad (3)$$

Since only three node types exist and their proportions sum to one, a simple way to characterise the topology of the network is to use a triangular plot (Fig 2e) (Manzocchi, 2002; Sanderson and Nixon, 2015).

2.2 Networks as graphs

In two-dimensions, a trace map or image of a fracture network (Fig. 2b) can be divided into a system of nodes and branches (Fig. 2c), whose arrangement forms a ***graph***. There are many different types of graph. If the branches are simple lines, with no implied sense of direction, the graph is termed an ***undirected graph***, whereas, if the linkage is in only one direction we have a ***directed graph.*** A ***simple graph*** is one where nodes are connected by single undirected branches (e.g., Fig. 2d), with no loops (branches starting and ending at the same node) or multi-branches (more than one branch between a pair of nodes). Most fracture networks are simple (undirected) graphs, although streamlines in fluid flow would be directed.

Any traverse along a sequence of adjacent nodes (i.e., nodes connected by branches) is termed a ***walk***, with a ***path*** being a walk that does not repeat a node and, hence, any branch. A ***cycle*** is a path that begins and ends at the same node. In addition to the nodes and branches, we can recognise two other elements - ***regions*** and ***components*** (Fig 2d). A ***connected component*** is a cluster of connected nodes, having at least one path between all pairs of nodes (as i-iv in Fig. 2d). A ***region*** is an area that is bounded by a cycle that does not have any other cycles embedded within it (shaded areas Fig. 2d). In a two-dimensional fracture network, the branches represent the fracture traces and the nodes their intersections, with the regions representing the (rock) material between the fractures and not the fracture surface (or 'face'). In section 4.5, we will elaborate further on the relationship between two- and three-dimensional networks. As an example of a two-dimensional graph (Fig. 2a), the tectonic plates are represented by regions in the graph, with plate boundaries as branches and triple junctions as nodes.

This definition of a *region* differs somewhat from the term ***face***, which is more commonly used in graph theory. The usage of *face* derives from Euler's study of polyhedra (Fig. 2b) that, when projected onto a plane, form a simple connected graph with faces that include one outer

surrounding face. The number of regions (|R|) is simply the number of faces (|F|) minus the outer face, hence, |R| = |F| - 1.

We have a number of reasons for our usage of the term region. 1) In a two-dimensional fracture network a fracture is represented by a series of branches forming its trace, the nodes represent the tips or edges of the fractures and their intersections. The regions then represent the blocks of rock between fractures. 2) For a simple connected graph, the regions are easily identified and are associated with a specific component (e.g., shaded in Fig 2d), whereas the 'outer face' (unshaded region in Fig. 2d) may be shared by many components.

2.3 Planar graphs

Since the node/branch model has nodes at all crossing points, it is a planar graph, i.e. can be drawn on a plane with branches that only cross at a node. Many large graphs, such as flight networks and the World-Wide Web, are non-planar because they have branches (flights, hyperlinks) between nodes (airports, webpages) that cannot be drawn on a plane without crossing. Planar graphs, and hence two-dimensional fracture networks, have some special properties that allow us to develop a range of relationships and metrics. In this section, we outline some techniques that we have found useful, but it must be emphasised that they just represent some initial steps into a wide range of potential applications and developments.

For example, in a connected planar graph, the maximum ($|B|_{max}$) and minimum ($|B|_{min}$) number of branches is given by (e.g. Wilson 1996):

$$|B|_{max} = 3|N| - 6 \quad (\text{or } |B|_{max} \approx 3|N|, \text{ as } |N| \rightarrow \infty) \qquad (4)$$

$$|B|_{min} = |N| - 1 \qquad (5)$$

Thus we would expect to find between 1 and 3 times as many branches as nodes in a connected fracture network.

2.4 Degree of a node

A basic metric for a node is its ***degree***, which is the number of adjacent branches. An I-node has d = 1, a Y-node has d = 3, and an X-node has d = 4. Natural fracture networks are dominated by low degree nodes (d ≤ 4), with only very occasional exceptions. Since all nodes have an associated degree, we can summarise these by the distribution of degree and associated metrics. The ***average degree <d>*** for a fracture network would lie between <d> = 1 (a network with only isolated fractures and I-nodes) and <d> = 4 (a network comprising a mesh of cross-cutting lines of infinite length, with all intersections represented by X-nodes). Figure 2e shows how <d> relates to the topology of the

network as expressed by the proportions of different nodes. <d> is a property that can be determined for any graph, i.e., not just one with I-, Y- and X-nodes.

Since each branch has 2 nodes, it follows that the average degree <d> is:

$$\langle d \rangle = 2|B|/|N| \quad (6)$$

This equation allows us to relate the number of branches and nodes, through what is widely referred to as the *handshaking lemma*. A handshake represents a relationship (branch) between two people (nodes), hence, for a finite group, the average number of handshakes per person is given by equation (6). In mathematics a lemma is a proof that is not important in its own right, but leads to other important proofs.

The handshaking lemma (equation 6) allows us to relate |N| and |B| through <d>, but there is a more fundamental relationship between them and the number of regions (|R|) and components (|K|). This relationship was discovered by Euler (1758) from his study of polyhedra, which may be represented as connected planar graphs, with the regions and the outer area of each graph representing a face, F (Fig. 2b). ***Euler's formula*** states that:

$$|N| - |B| + |F| = 2 \quad (7)$$

Substituting $|F| = |R| + 1$ gives:

$$|N| - |B| + |R| = 1 \quad (8)$$

where the right hand side (= 1) represents the number of components |K|, thus the ***generalisation of Euler's formula*** to multicomponent networks may be written as:

$$|N| - |B| + |R| - |K| = 0 \quad (9)$$

Since each node, branch and region belongs to only one component (Fig. 2d), we can sum the values of each component to get metrics for the entire graph. This is another reason for using |R| rather that |F| in equation (9), which is a key to the analysis of large, multi-component, natural fracture networks.

2.5 Large planar graphs (LPGs)

Most fracture networks are made up of components of very large size, and many continue well beyond the region of investigation. For example, an exposed rock surface is just part of a larger rock volume and has many fractures that continue beyond its limits. They form Large Planar Graphs (LPGs) that may consist of any number of connected components of differing size (Fig. 3). So a key issue is how we might relate nodes, branches, regions and components in a sample of such a graph, i.e., a map or image of part of a fracture network.

Figure 3a shows a very simple version of an LPG, with only 3 components, two of which continue out of the sample circle. Using only information from within the circle, what can we deduce about the graph? Node counting gives |I| = 10, |Y| = 10, |X| = 1 and, hence, |N| = 21 (equation 1), |B| = 22 (equation 2) and <d> = 2.10 (equation 6). Note that there are 24 branches in Fig 3a, of which $|B_C|$ = 20 are entirely within the circle, with four more continuing out of the circle to produce |E| = 4. Effectively the branches that continue out of the circle count as ½ or:

$$|B| = |B_C| + |E|/2 \qquad (10)$$

There is one component (A) completely within the circle and up to 2 extending beyond. We do not know if B and C are connected outside the circle, but this uncertainty sets a lower and upper bound to |K|, for which we may calculate corresponding values for |R| using Euler's formula (equation 9).

In cases where E-nodes are linked within the sample area, as in the joint network in Figure 3b, we know the number of components |K| and can use Euler's formula (equation 9) to find the number of regions |R|. From Figure 3c, |K| = 1, |N| = 21 and |B| = 26 + |E|/2 = 31.5, and, using equations 9, the number of regions |R| = 31.5 – 21 + 1 = 11.5. This value for |R| includes the complete-regions, within a closed circuit of branches and nodes, as well as 'half'-regions which leave the sample area.

2.6 Spatially referenced (Eulerian) graphs

So far, the properties of LPGs have been considered as independent of the spatial position of the nodes and branches. A trace map or image of a fracture system can be considered as a specific drawing of a graph. Thus, the topology of the graph is combined with the geometry through spatial referencing. We can consider two levels:

(1) By locating nodes in their correct spatial positions, the branches formed by straight lines between these nodes will provide a minimum length and average orientation of the fracture traces.

(2) Digitising each branch as a polyline more accurately represents its length and shape. This approach allows extraction of more complex branch features, such as sinuosity or orientation variance. The extra nodes in the polyline may be discarded in the topological analysis of the graph.

The degree to which (2) is a significant advance on (1) depends on the details of the fracture geometry, resolution of the imaging and aims of the project. A study of caves in a karst system by Collon et al. (2017) provides a practical discussion of many of these issues. For many applications, it may be both adequate and efficient to spatially register only the nodes to capture the main features of a fracture network.

Detailed images of fracture systems are easily and rapidly acquired from aerial photography (e.g., Nixon et al., 2011; Bemis et al., 2014), UAV images (Vasuki et al., 2014), satellite images (e.g., Zeeb et al., 2013), sonar bathymetry (e.g., Nixon et al., 2012; Sanderson et al., 2017), Lidar (e.g., Rotevatn et al., 2009), etc. In addition, trace maps made in the field are routinely digitised (e.g. Dimmen et al., 2017), with GIS packages allowing a range of input methods and analysis techniques (e.g., Healy et al., 2017). A comprehensive account of how a GIS may be used to extract useful topological data is given by Nyberg et al. (in press). Indeed, the extraction of topology, as outlined in section 2, is usually much simpler than that of geometry, e.g., determining lengths and orientations of lines, construction of rose diagrams and stereograms (see also Procter and Sanderson 2017).

3. Characterisation of networks

3.1 Topological classification of networks

Topology describes the relationship between fractures and, as such, adds information for the characterisation of a network. For most fracture networks, the nodes are either I, Y or X, and the proportion of each provides a basis for describing the topology (Sanderson and Nixon 2015). From Fig. 2e, isolated and poorly-connected networks plot towards the I vertex of the triangle, whereas well-connected mesh-like networks plot closer to the Y-X side, with polygonal and cross-joint systems being dominated by Y-nodes and cross-cutting systems by X-nodes. Graph metrics, such as <d> can be plotted on the same triangular diagram by combining equations (1), (2) and (6). On the rare occasions where other node types are present, the graph metrics still provide information on the topology, and can be estimated even with limited access to the network as a whole.

3.2 Workflows in network characterisation

Several recent studies have incorporated aspects of topology in the analysis of fault networks (Nixon et al., 2011, 2012; Duffy et al., 2017) and joint systems (Watkins et al., 2015a, b). Procter and Sanderson (2017) propose a workflow for analysis of fracture networks that is based on node counting within a circle of known area. They also recommend digitising and rectification in GIS to produce a spatial graph suitable for extraction of other topological and geometrical data (Fig. 4a, b).

Where the sample area is a circle, the fracture intensity (I) can be determined from the edge intersections (|E|) as described by Mauldon et al. (2001), with the resulting fracture intensity (P_{10}) being in good agreement with that obtained from two-dimensional trace mapping (P_{21}):

$$P_{10} = P_{21} = (|E| / 2 \pi r) . \pi/2 = |E| / (4 r) \quad (11)$$

Procter and Sanderson (2017) argue that determination of fracture intensity is ~ 10 times faster than by traditional field mapping, thus greatly improving the efficiency of fracture studies.

3.3 Ages, sets and types of fractures

The abutting relationship at Y-nodes provides key evidence for the relative age of faults and joints (Hancock, 1985; Sanderson, 2015). For example, Fig. 4c shows a network dominated by Y-nodes, with three of the red fractures (later) abutting against two of the blue fractures (earlier) (Fig. 4d). The remaining green fractures all abut against either the red or blue fractures (Fig. 4e), indicating that they are the latest to form. The type and relative age of fractures are not directly related to their geometry and, together with the orientation (geometry) are key components in the definition of different fracture sets. Procter and Sanderson (2017) use the abutting relationships to establish a fairly consistent order of development of the joint sets (as Fig. 4d, e). They also showed that a small proportion of the Y-nodes indicated the repeated development of cross-joints between more closely spaced, earlier joints (c.f. Bai et al., 2002) at different stages in the development of the network.

Many structures involve combinations of different fracture types, as in the shear zone in Fig. 5a. The proportions of node types in fault networks (e.g. Fig. 5b) and associated graph metrics have been shown to vary systematically during the evolution of multi-phase rifts (Duffy et al., 2017) and with the resolution of mapping of conjugate fault arrays (Nixon et al., 2012).

3.4 Regions and compartments

In section 2.4, we discussed how the number of regions |R| in a network can be determined using Euler's formula. If the area occupied by the network is known, then the average block area can be calculated. In the example in Fig. 3c, the average block area is estimated to be 0.04 m^2 (Fig. 3d), which agrees closely with the observed sizes of complete block (Fig. 3c). Similar calculations on fault networks (Fig. 5c) can be used to estimate fault-bound compartments in hydrocarbon reservoirs (Nixon et al., 2017).

This type of estimate is important, particularly in petroleum industry where there has been much work on the identification and assessment of reservoir compartments (e.g., Bouvier et al., 1989; Smalley and Hale, 1996; Manzocchi et al., 2010; Go et al., 2012). It can also be applied to determine the block size in the evaluation of fluid exchange between matrix and fractures in fractured reservoirs.

4. Recent and future developments

In this section, we discuss some recent developments on networks that are based on graph theory, and indicate potential future applications.

4.1 Weighted graphs

A *weighted graph* is a graph in which values (weights) are attached to the branches and/or nodes. A simple example is in a SatNav system, where data are stored as lists of nodes (locations) and branches (roads). If distances, traffic conditions, etc. are values associated with each branch, then routes may be calculated and algorithms exist to extract shortest and quickest paths.

A branch is specified by a pair of nodes, but additional information could be added, such as the type of fracture (e.g., fault, opening-mode fracture, deformation band, etc.). It may also be helpful to attach labels to identify connected or isolated branch types (Sanderson and Nixon 2015) and length or orientation of fractures, although some can be estimated from the associated nodes. We can also attach fracture attributes to each branch: width (thickness, aperture), displacement or separation (throw, heave) of a fault (Fig. 5d), permeability, or an age or set identifier. Some quantities may be estimated, such as conductance or sinuosity. For active faults, we could also store information about slip-rates, earthquake events, magnitudes and recurrence times.

A node will usually be identified by a name or number, together with a location (x, y coordinates) if we are describing a spatial graph. For some applications it is useful to store the node type or degree, although these may be estimated from the associated branches. For example, in Fig. 5d regions of high average degree correspond to areas of interacting conjugate faults and resultant damage. In some cases, it may be useful to assign further information concerning the type of intersection, e.g. where flow is concentrated at nodes, especially for faults (e.g. Peacock et al., 2017)).

A simple, but effective, use of weights is to display their distribution on the network, either by extracting different fracture types and/or displaying the distribution of attribute values across the network. A simple example is shown in Figure 5a, where a pull-apart array (i) is separated into fault components (ii) and en echelon veins (iii), with the thickness of the veins being related to the pull-aparts developed between the faults. Qualitative information such as separation and vein thickness could be represented, and contoured, if appropriate, to show spatial variation (e.g. Procter, et al., 2017). It is also possible to extract and manipulate the attributes, which leads to applications ranging from the length weighting of orientation data to displacement and length weighting of fault sets (e.g., Nixon et al., 2011).

4.2 Databases and graph processing algorithms

In computer science, the graph structure can be used to represent many different types of data and to solve a wide range of combinatorial problems (e.g., Gibbons, 1988; Kocay and Kreher, 2017). They include routines to search for connected components and paths between nodes, such as the shortest path. An important step in utilising these algorithms is to realise that they are built around lists of nodes and branches (section 2.1). The interpretation of fracture networks has traditionally involved the mapping of fracture traces and the measurement of fracture orientation. Orientation data are usually plotted on stereograms and rose diagrams and, hence, divorced from their absolute and relative positions. Digitising of field maps creates polylines that preserve the spatial position of the data, but are often not tied (or snapped) to the nodes or intersections, hence their relationships are poorly determined. The solution is simple in a GIS: start by generating the nodes, then draw the traces as lines snapped to these nodes. It is then possible to attach additional data (e.g., fault throws, vein thicknesses, mineral concentrations) directly to the branches and nodes. Thus, the graph serves as a relational database. Automatically taking data from imagery and generating a graph is a much harder problem, although a range of software tools are available, including several integrated into GIS packages. Other problems that could make explicit use of graph structures include: evaluation of connectivity and cluster size distribution; displacement, slip-rate and seismic hazard analysis on fault networks; thickness and grade evaluation in mineral veins.

4.3 DFNs and geomechanics

The graph has a system of branches that are tied to nodes and, hence, provides a robust basis for generating computational networks and meshes in a range of numerical models in geomechanics. The branches define a Discrete Fracture Network (DFN) with the nodes ensuring no gaps between fractures. The regions define discrete elements, with branches defining contacts between these elements, the basis for Distinct Element Models (e.g., Zhang and Sanderson 2002; Jing and Stephansson 2007). The network also forms a mesh, suitable as a basis for Finite Element Models (FEM), with further meshing possible within regions and by subdivision of the branches (e.g., Edelsbrunner 2001). The graph is also the basic structure required for network flow calculations, with the branches having specific conductance and nodes providing the basis for the pressure distribution (e.g., Zimmerman and Bodvarsson, 1996).

4.4 Connectivity, percolation and permeability

Metrics derived from graph theory and topology have particular relevance to the assessment of connectivity in fracture networks (Manzocchi, 2002; Sanderson and Nixon, 2015). Counting nodes and branches allow the calculation of metrics that help describe to what degree a network is

connected, such as average degree, connections per branch and connections per line. In addition, graph processing algorithms allow us to extract the largest connected component, the size of which ultimately determines if a cluster spans the sample area and, hence, if the system has reached a percolation threshold. Some advances have been made in assessing connectivity by linking metrics to known and simulated models (e.g., Manzocchi, 2002). This is a difficult problem as the value of the metrics are known to depend on the network topology (Sævik and Nixon, 2018; Sanderson and Nixon, in prep.).

Network connectivity is particularly important when estimating the effective permeability of fractured rock masses, an important parameter when simulating fluid flow. Discrete fracture network models or conceptual models, based on measured geometric data from boreholes or outcrop analogues, are often used to estimate the effective permeability and can then be calculated using analytical methods (e.g., Oda, 1985; Mourzenko et al., 2011) or numerical upscaling (e.g., Karimi-Fard et al., 2006). One problem with this approach is that the random placement of fractures of specified geometry does not preserve the graph properties of the natural network (e.g., connectivity). Better results can be achieved through analytical upscaling whereby a functional relationship between fracture parameters and the effective permeability is used. Sævik and Nixon, (2018) have used topological measures of connectivity to produce improved permeability estimates.

The network may also evolve over time, as in Fig. 4, with changing and superposed stress fields leading to fracture propagation (e.g. Olsen et al. 2009; Duffy et al 2017). In addition, important aspects of an existing network may change, for example by opening and closure of fractures (e.g. Zhang and Sanderson, 1998; 2002), with fluid flow leading to dissolution or cementation (e.g. Alzayer et al., JSG, 2015; Hooker et al., JSG, 2017; Laubach et al. 2018).

4.5 Three-dimensional networks and associated topology

Traditionally much of the data for fracture networks has been from surfaces (maps, imaged surfaces, etc.) and is essentially two-dimensional. Note that surface mapping and use of Lidar allows us to extract three-dimensional information, but we are still essentially sampling a surface. Seismic volumes of faults and CT scanning of smaller fractures allow increasing access to three-dimensional data, so how can we extend the graphs and topology to three-dimensions? It is obvious that fractures (branches) then become planes, tips and intersections (nodes) become lines, and rock blocks (regions) become polyhedra. Whilst a full three-dimensional analysis of fracture networks remains a major challenge for future research, some simple steps can be made that we illustrate in Figure 6.

Figure 6a shows a very simple network with three fractures within a cube that produce traces on the surfaces. The upper surface (Fig. 6b) represents a trace map, the other two faces (6c, d) can be thought of as cross-sections (cliff profiles, seismic sections, etc.). The three faces of the cube will generally produce somewhat different graphs, with different two-dimensional network topologies (Fig. 6e). Here we examine three simple steps towards a more three-dimensional analysis.

1) We could simply average the results from different sections through the three-dimensional volume. The degree to which the sections provide information about the three-dimensional volume is a common problem in stereology (e.g. Underwood 1970). Combining the node counts from the three sections produces an average shown by the filled circle in Fig. 6e.

2) Where observation is restricted to a single surface, we can improve our estimate of the three-dimensional topology by recognising that the probability of a plane or line intersecting the surface depends on its dip (δ) or plunge (α), respectively. Terzaghi (1965) proposed a correction or weight ($1/\sin(\delta)$ or $1/\sin(\alpha)$) which is widely used in fracture studies. Note that where δ or α are 90° these correction factors are 1, as occurs for bedding planes with orthogonal fracture sets.

3) At the level of individual blocks (polyhedra), we can develop the approach of Euler (Fig. 2b), but this approach awaits further investigation.

The effect of (1) and (2) is to provide a more representative measure of network topology, but many sampling issues exist (see e.g. Priest 1993), and the methods are not easily applied to analysis of regions and components. Clearly, much future work needs to be done to develop the analysis of three-dimensional networks.

5. Conclusions

By stepping back, both in time and philosophy, we argue that the future development of fracture network analysis can be strongly influenced by graph theory that started way back in 1736 with Euler. Fracture networks of all types and scales can be characterised in terms of their topology rather than their geometry. In two-dimensions, a fracture network can be seen as a system of branches and nodes. These elements form a planar graph, since all crossings of fractures are nodes. Simple application of graph theory allows us to generalise the node/branch model, which opens up a range of approaches, many of which have been developed in other disciplines. We start to see parallels with the analysis of other types of network (Table 1), e.g. urban street networks share many of the features of fault networks, being dominated by low degree (X and Y) nodes.

410 This approach to networks both enriches and extends the scope of more traditional geometrical
411 techniques. Key developments include:

412 1) Fracture networks can be treated as large planar graphs (LPG) that comprise a series of
413 nodes (N), linked by branches (B), which bound regions (R), to form connected components
414 (K). These quantities can thus be counted and used to characterize the network in terms
415 other than that of the geometry of the component fractures.

416 2) Almost all nodes in fracture networks have degree 1 (I-nodes), 3 (Y-nodes) or 4 (X-nodes),
417 so that the proportions of these node types provide a basis for characterizing the topology
418 of the network.

419 3) The average degree <d> relates the number of branches (|B|) and nodes (|N|) through the
420 relationship |B| = ½<d>|N| (the handshaking lemma). Thus, counting nodes can be used to
421 determine the number of branches, which simplifies network analysis.

422 4) Euler's formula establishes a link between all four elements of the graph with |N| - |B| +
423 |R| - |K| = 0.

424 5) Since it is not often possible to observe or sample the entire fracture network, we need to
425 consider how best to sample an LPG to extract information on elements such as block size,
426 and number and size of components.

427 Treating fracture networks as a graph opens up a wide range of applicable theorems, which we have
428 only just begun to utilize. Graph theory is widely used in computer science where graphs provide a
429 key data structure and are used to solve a wide range of combinatorial problems. Thus, many
430 efficient algorithms already exist to aid the analysis of fault and fracture systems, but, to date, little
431 use has been made of them.

432

433 ## 6. Acknowledgements

434 Nixon is supported by a VISTA scholarship (project no. 6265) from the Norwegian Academy of
435 Science and Letters and Sanderson by a Leverhulme Emeritus Fellowship. We thank the journal
436 reviewers (Mark Fisher and an anonymous reviewer) and editor (Bill Dunne) for their useful and
437 considered reviews that have helped improve the manuscript.

7. References

Agricola, G., 1556. De re metallica. Translated by Hoover, H.C., Hoover, L.H., 1998. Dove, New York, 638pp.

Alzayer, Y., Eichhubl, P., Laubach, S.E., 2015. Non-linear growth kinematics of opening-mode fractures. Journal of Structural Geology 74, 31-44.

Bai, T., Maerten, L., Gross, M.R., Aydin, A. 2002. Orthogonal cross joints: do they imply a regional stress rotation? Journal of Structural Geology 24, 77-88.

Bemis, S.P., Micklethwaite, S., Turner, D., James, M.R., Akciz, S., Thiele, S.T., Bangash, H.A., 2014. Ground-based and UAV-based photogrammetry: A multi-scale, high-resolution mapping tool for structural geology and paleoseismology. Journal of Structural Geology 69, 163-178.

Bondy, J.A., Murty, U.S.R., 2008. Graph Theory, Springer, ISBN 978-1-84628-969-9.

Bouvier, J., Kaars-Sijpesteijn, C., Kluesner, D., Onyejekwe, C., van der Pal, R., 1989. Three-dimensional seismic interpretation and fault sealing investigations, Nun River Field, Nigeria. AAPG Bulletin, 73, 1397–1414.

Collon, P., Bernasconi, D., Vuilleumier, C., Renard, P., 2017. Statistical metrics for the characterization of karst network geometry and topology. Geomorphology 283, 122–142.

Dimmen, V., Rotevatn, A., Peacock, D.C., Nixon, C.W., Nærland, K., 2017. Quantifying structural controls on fluid flow: insights from carbonate-hosted fault damage zones on the Maltese Islands. Journal of Structural Geology 101, 43-57.

Duffy, O.B., Nixon, C.W., Bell, R.E., Jackson, C.A.L., Gawthorpe, R.L., Sanderson, D.J. and Whipp, P.S., 2017. The topology of evolving rift fault networks: Single-phase vs multi-phase rifts. Journal of Structural Geology, 96, 192-202.

Edelsbrunner, H., 2001. Geometry and topology for mesh generation. Cambridge University Press 183pp.

Euler, L. 1736. Solutio problematis ad geometriam situs pertinentis. Access through http://eulerarchive.maa.org (article 53).

Euler, L. 1758. Elementa doctrinae solidorum. Access through http://eulerarchive.maa.org (article 230).

Gibbons, A., 1988. Algorithmic Graph Theory. Cambridge University Press.

Go, J., Smalley, P. C., Muggeridge, A. 2012. Appraisal of reservoir compartmentalization using fluid mixing time-scales: Horn Mountain Field, Gulf of Mexico. Petroleum Geoscience, 18, 305–314.

Hancock, P.L. 1985. Brittle mictotectonics: principles and practice. Journal of Structural Geology 7, 437-457.

Healy, D., Rizzo, R.E., Cornwell, D.G., Farrell, N.J., Watkins, H., Timms, N.E., Gomez-Rivas, E., Smith, M., 2017. FracPaQ: a MATLAB™ toolbox for the quantification of fracture patterns. Journal of Structural Geology 95, 1–16.

Hooker, J.N. Laubach, S.E. Marrett, R., 2018. Microfracture spacing distributions and the evolution of fracture patterns in sandstones. Journal of Structural Geology 108, 66-79.

Jing, J., Stephansson, O., 1994. Topological identification of block assemblages for jointed rock masses. Int. J. Rock Mech. Min. Sci. & Geomech. Abstr. 31, 163-172.

Jing, L., Stephansson, O., 1997. Network topology and homogenization of fractured rocks. In: Jamtveit, B., Yardley, B.W. (Eds.), Fluid Flow and Transport in Rocks. Mechanisms and Effects. Chapman & Hall, Oxford, pp. 191-202.

Jing, J., Stephansson, O., 2007. Fundamentals of discrete element methods for rock engineering: theory and applications. Elsevier 545pp.

Karimi-Fard, M., Gong, B., Durlofsky, L.J., 2006. Generation of coarse-scale continuum flow models from detailed fracture characterizations. Water Resources Research, 42, W10423.

Kocay, W.L., Kreher, D.L., 2017. Graphs, Algorithms and Optimization (2nd edition), CRC Press 545 pp.

Laubach, S.E., Lamarche, J., Gauthier, B.D.M., Dunne, W.M., Sanderson, D.J., 2018. Spatial arrangement of faults and opening-mode fractures. Journal of Structural Geology, 108, 2-15.

Manzocchi, T., 2002. The connectivity of two-dimensional networks of spatially correlated fractures. Water Resources Research 38, 1162.

Manzocchi, T., Childs, C., Walsh, J.J., 2010. Faults and fault properties in hydrocarbon flow models. Geofluids, 10, 94–113.

Mauldon, M., Dunne, W.M., Rohrbaugh Jr., M.B. 2001. Circular scan lines and circular windows: new tools for characterizing the geometry of fracture traces. Journal of Structural Geology 23, 247–258.

Mourzenko, V.V., Thovert, J.F., Adler, P.M., 2011. Permeability of isotropic and anisotropic fracture networks, from the percolation threshold to very large densities. Physical Review E, 84, 036307.

497 Nixon, C.W., Sanderson, D.J., Bull, J.M., 2011. Deformation within a strike-slip fault network at
498 Westward Ho! Devon U.K.: domino vs conjugate faulting. Journal of Structural Geology 33, 833–
499 843.

500 Nixon, C.W., Sanderson, D.J., Bull, J.M., 2012. Analysis of a strike-slip fault network using high
501 resolution multibeam bathymetry, offshore NW Devon U.K. Tectonophysics 541–543, 69-80.

502 Nixon, C.W., Sanderson, D.J., Dee, S., Bull, J.M., Humphreys, R., Swanson, M., 2014. Fault
503 interactions and reactivation within a normal fault network at Milne Point, Alaska. AAPG
504 Bulletin 98, 2081-2107.

505 Nyberg, B., Nixon, C.W., Sanderson, D.J., 2018. NetworkGT: a GIS tool for Geometric and Topological
506 Analysis of two-dimensional Fracture Networks. Geosphere, in press.

507 Oda M., 1985. Permeability tensor for discontinuous rock masses. Geotechnique 35, 483–495

508 Olson, J.E., Laubach, S.E., Lander, R.H., 2009. Natural fracture characterization in tight gas
509 sandstones: integrating mechanics and diagenesis. AAPG Bulletin, 93, 1535-1549.

510 Peacock, D.C.P., Nixon, C.W., Rotevatn, A., Sanderson, D.J., Zuluaga, L.F., 2016. Glossary of fault and
511 other fracture networks. Journal of Structural Geology 92, 12–29.

512 Peacock, D.C.P., Dimmen, V., Rotevatn, A., Sanderson, D.J., 2017. A broader classification of damage
513 zones. Journal of Structural Geology 102, 179-192.

514 Pollard, D.D., Aydin, A., 1988. Progress in understanding jointing over the past century. Geological
515 Society of America Bulletin 100, 1181-1204.

516 Priest, S.D., 1993. Discontinuity Analysis for Rock Engineering. Chapman & Hall, New York, 473 pp.

517 Procter, A., Sanderson, D.J., 2017. Spatial and layer-controlled variability in fracture networks.
518 Journal of Structural Geology doi.org/10.1016/j.jsg.2017.07.008.

519 Rotevatn, A., Buckley, S.J., Howell, J.A., Fossen, H., 2009, Overlapping faults and their effect on fluid
520 flow in different reservoir types: a LIDAR-based outcrop modelling and flow simulation study.
521 AAPG Bulletin 93, 407-427.

522 Sanderson, D.J., 2015. Field-based structural studies as analogues to sub-surface reservoirs. In:
523 Bowman, M., Smyth, H.R., Good, T.R., Passey, S.R., Hirst, J.P.P., Jordan, C.J. (Eds.), The Value of
524 Outcrop Studies in Reducing Subsurface Uncertainty and Risk in Hydrocarbon Exploration and
525 Production. Geological Society London, Special Publications 436,
526 http://dx.doi.org/10.1144/SP436.5.

527 Sanderson, D.J., Nixon, C.W., 2015. The use of topology in fracture network characterization. Journal
528 of Structural Geology 72, 55-66.

529 Sanderson, D.J., Nixon, C.W., 2017. Topology, connectivity and percolation in fracture networks.
530 Journal of Structural Geology (in revision).

531 Smalley, P.C., Hale., N.A. 1996. Early identification of reservoir compartmentalization by combining a
532 range of conventional and novel data types. SPE Formation Evaluation, 11(3), 163–170.

533 Sævik, P.N., Nixon, C.W., 2018, Effective permeability of fractured rock from topological
534 measurements. Water Resources Research, in press.

535 Terzaghi, R.D. 1965. Sources of error in joint surveys. Geotechnique 15, 287-304.

536 Underwood, E.E., 1970. Quantitative Stereology, Addison-Wesley Publishing Co., Reading, MA.

537 Vasuki, Y., Holden, E.J., Kovesi, P., Micklethwaite, S., 2015. Semi-automatic mapping of geological
538 Structures using UAV-based photogrammetric data: an image analysis approach. Computers
539 and Geoscience 69, 22-32.

540 Watkins, H., Bond C.E., Healy D., Butler, R.W.H., 2015a. Appraisal of fracture sampling methods and
541 a new workflow to characterise heterogeneous fracture networks at outcrop. Journal of
542 Structural Geology 72, 67-82.

543 Watkins, H., Butler, R.W.H., Bond C.E., Healy D., 2015b. Influence of structural position on fracture
544 networks in the Torridon Group, Achnashellach fold and thrust belt, NW Scotland. Journal of
545 Structural Geology 74, 64-80.

546 West, D.B., 1996. Graph Theory. Prentice Hall, New Jersey,

547 Wilson, R.J., 1996. Introduction to Graph Theory (2nd edition). Addison Wesley Longman, Harlow 171
548 pp.

549 Zeeb, C., Gomez-Rivas, E., Bons, P.D., Blum, P., 2013. Evaluation of sampling methods for fracture
550 network characterization using outcrops. American Association of Petroleum Geologists
551 Bulletin, 97, 1545-1566.

552 Zhang, X., Sanderson, D.J. 1998. Numerical study of critical behaviour of deformation and
553 permeability of fractured rock masses. Marine & Petroleum Geology, 15, 535-548

554 Zhang, X., Sanderson, D.J. 2002. Numerical Modelling and Analysis of Fluid Flow and Deformation of
555 Fractured Rock Masses. Pergamon 288pp.

556 Zimmerman, R.W., Bodvarsson, G.S., 1996. Effective transmissivity of two-dimensional fracture
557 networks. Int. J. Rock Mech. Min. Sci., 33, 433-438.
558

Figure Captions

Figure 1 (a) Examples of networks of mineral veins at earth's surface, from Agricola (1556). (b) Interpretation of these examples using node / branch model;

(c) Node/branch model (after Sanderson and Nixon 2015) where a fracture trace (A-B) is divided into branches, with a node at each end. The nodes represent fracture tips (green circles), abutting fractures (red triangles) or cross-cutting intersections (blue squares).

(d) Schematic diagram of a three-dimensional fracture network showing fracture faces (hatched), tips and intersections (lines), and vertices (yellow circle). These intersect the surfaces of the cube to produce fracture traces (B – branches), with the tips and intersection lines producing points or nodes (annotated as Fig. 1c).

Figure 2 (a) Equal-area stereographic projection (whole sphere) of Earth, showing plate boundaries (lines), triple junctions (triangles) and tectonic plates (Af - African, An -Antarctic, Au - Australian, Ar – Arabian, EA – Eurasian, Ca – Carribean, Co - Cocos, JF – Juan de Fuca, In – Indian, N – Nazca, NA – North American, P – Pacific, Ph – Philippine, SA – South American, Sc - Scotia).

(b) Trace map of fracture network with four connected components (*i* – *iv*). (c) Node branch model of (b), notation as in Fig 1(c). (d) Graph representation of (b) showing the nodes (dots), branches (lines), regions (shaded) and components ((*i* – *iv*).

(e) Triangular plot of proportions of I, Y and X nodes, showing average degree (<d>) and examples of two-dimensional fracture networks plotting in different parts of the triangle.

Figure 3 (a) A simple graph with three components (A, B, C) as sampled within a circle. Dots are nodes, lines are branches, and stars are edge (E) nodes. Two regions (shaded) are associated with component B.

(b) Joint network exposed on a limestone bedding surface. (c) Interpretation as graph using notation in Fig. 3(a), with circles indicating regions within map area and semicircles indicating regions that extend beyond the edge of the photograph. (d) represents the average block area (0.04 m^2) and is drawn at same scale as in (b) and (c).

588 Figure 4 (a) Field photograph of a joint network that is normal to a bedding surface, with 2 m
589 diameter circle and north shown on bedding. (b) Rectified image of the joint network
590 (after Procter and Sanderson, 2017).

591 (c) Bedding surface with traces of joints, normal to bedding. (d) Later joints (red) abutting
592 earliest joints (blue) with example in circles. (e) Latest joints (green) abutting both earlier
593 sets.

594 Figure 5 (a) Shear zone in limestone, with *en echelon* faults (ii) and vein clusters (iii) combining to
595 produce linked shear zone (i).

596 (b) Part of fault network comprising conjugate sets of strike-slip faults cutting folded Upper
597 Carboniferous strata mapped on a bathymetric image from offshore, Hartland, north
598 Devon, UK (after Nixon et al., 2012). Nodes identified as in Figure 1c..

599 (c) Interpretation of seismic volume, from Milne Point, Alaska, showing compartments
600 (after Nixon et al., 2015).

601 (d) Part of strike-slip fault network from Westward Ho!, North Devon, UK (Nixon et al,
602 2011). Width of lines indicate fault displacement and colours indicate average degree
603 (<d>) of nodes, with high values corresponding to interconnected conjugate faults and
604 associated damage.

605 Figure 6 (a) Isometric projection of three intersecting fractures within a cube, with tip lines (green)
606 and intersection lines (dashed). Nodes (as in Fig. 1c) and branches (lines) are shown on
607 top and front surfaces of cube. (b) Upper surface of (a) showing simple graph, with plunge
608 of lines (α) and fracture dip (δ). (c) and (d) Similar plots for 2 sides of cube. (e) Triangular
609 plot of proportions of nodes on surfaces (b), (c) and (d), with average from aggregated
610 data on each surface (filled circle).

611

612

Tables

Table 1

Examples of graphs from range of disciplines. Most form planar graphs, with non-planar graphs indicated by (np) in Region column since concept does not apply.

This paper	NODE (point)	BRANCH (line)	REGION (area)	COMPONENT
Graph theory	vertex, node	edge (link)	face (region)	connected component
Fractures	Tip, intersection, cut-off	fracture trace (with fracture type where necessary)	block	component, cluster
Plate tectonics	triple junction	plate boundary	plate	planet
Micro-structure	dislocation	loop/line	slip-patch	grain
Chemistry	atom	bond	(np)	molecule, lattice
Geography	location (e.g., city, house)	border, road, etc.	country, county, block	City, country
	junction	river	catchment area	island, continent
	airport	flight	(np)	airline?
Computing	device (e.g., computer, server, printer)	cable, wire wifi	(np)	Local Area Network
	web page	hyperlink	Intranet?	World Wide Web
Sociology	person	friendship, handshake, etc.	(np)	isolated community or group (e.g., Facebook)
Business	person, unit, committee, etc.	reporting route	(np)	organisation

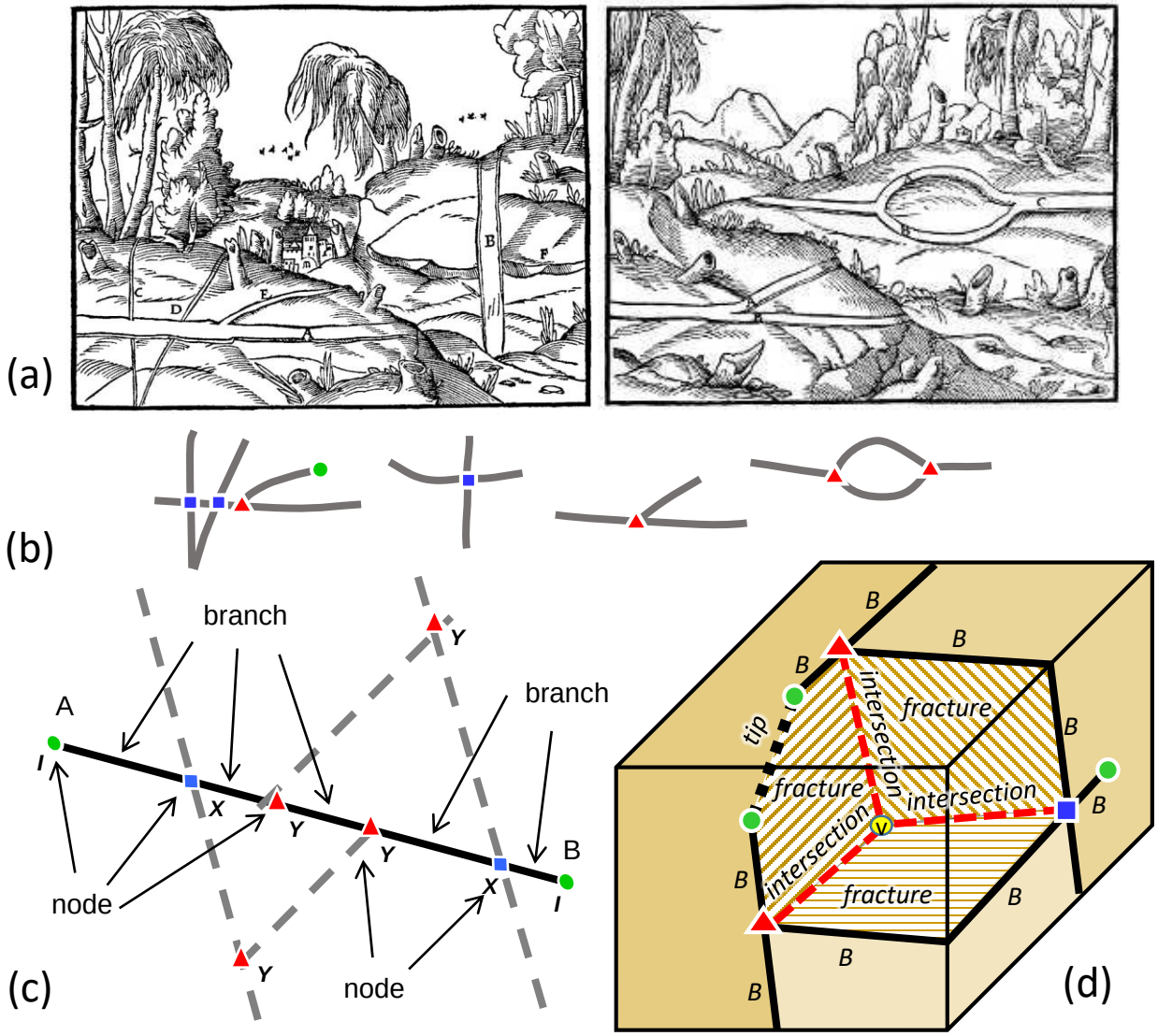
(a)
(b)
branch
branch
A
B
I
X
Y
node
node
(c)
B
tip
intersection
fracture
intersection
fracture
intersection
fracture
V
(d)

Figure 1

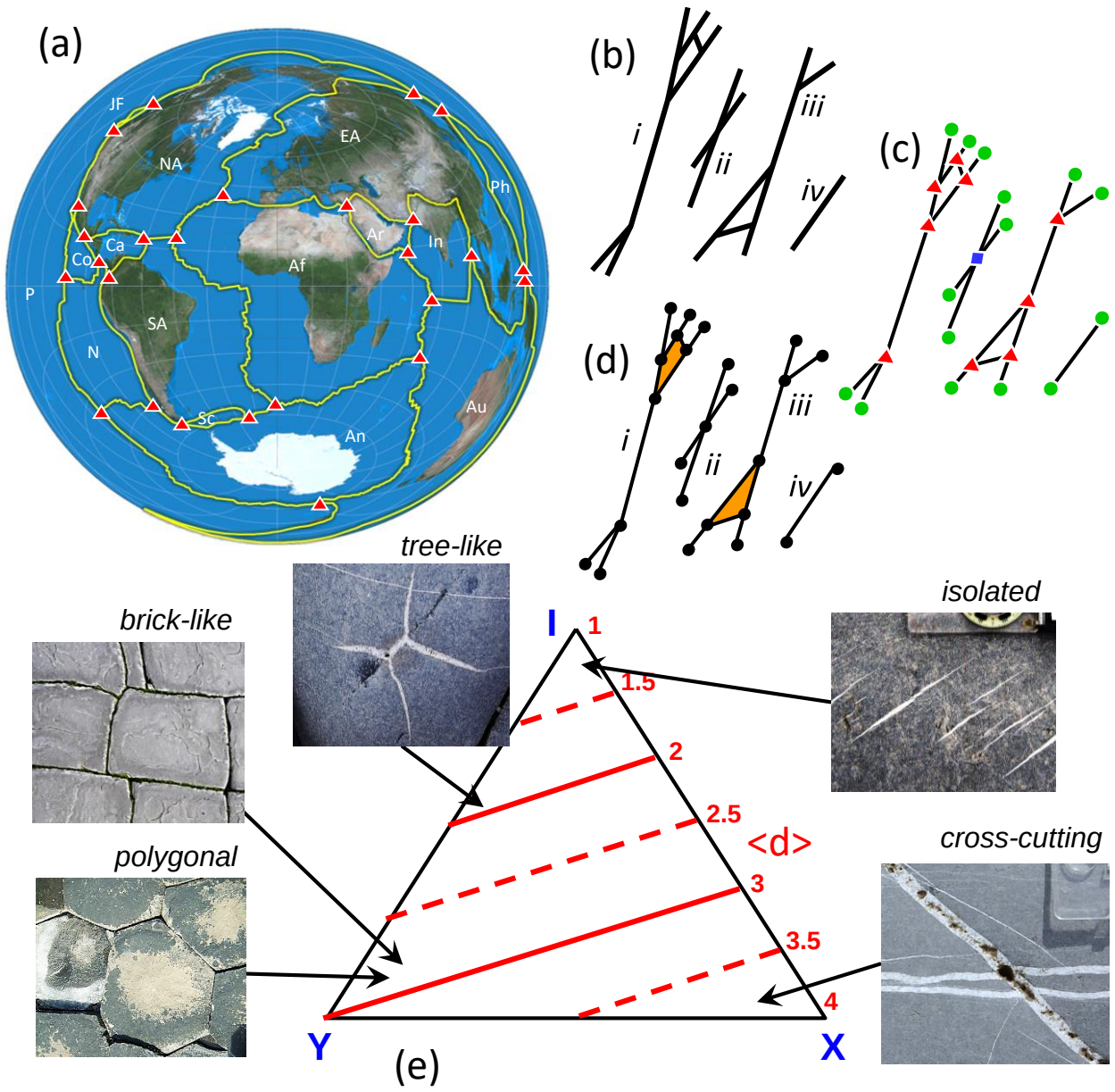
(a)
JF
NA
EA
Ph
Ar
In
Af
Ca
Co
P
SA
N
Sc
An
Au
(b)
i
ii
iii
iv
(c)
(d)
i
ii
iii
iv
tree-like
brick-like
isolated
polygonal
cross-cutting
I
1
1.5
2
2.5
<d>
3
3.5
4
Y
X
(e)

Figure 2

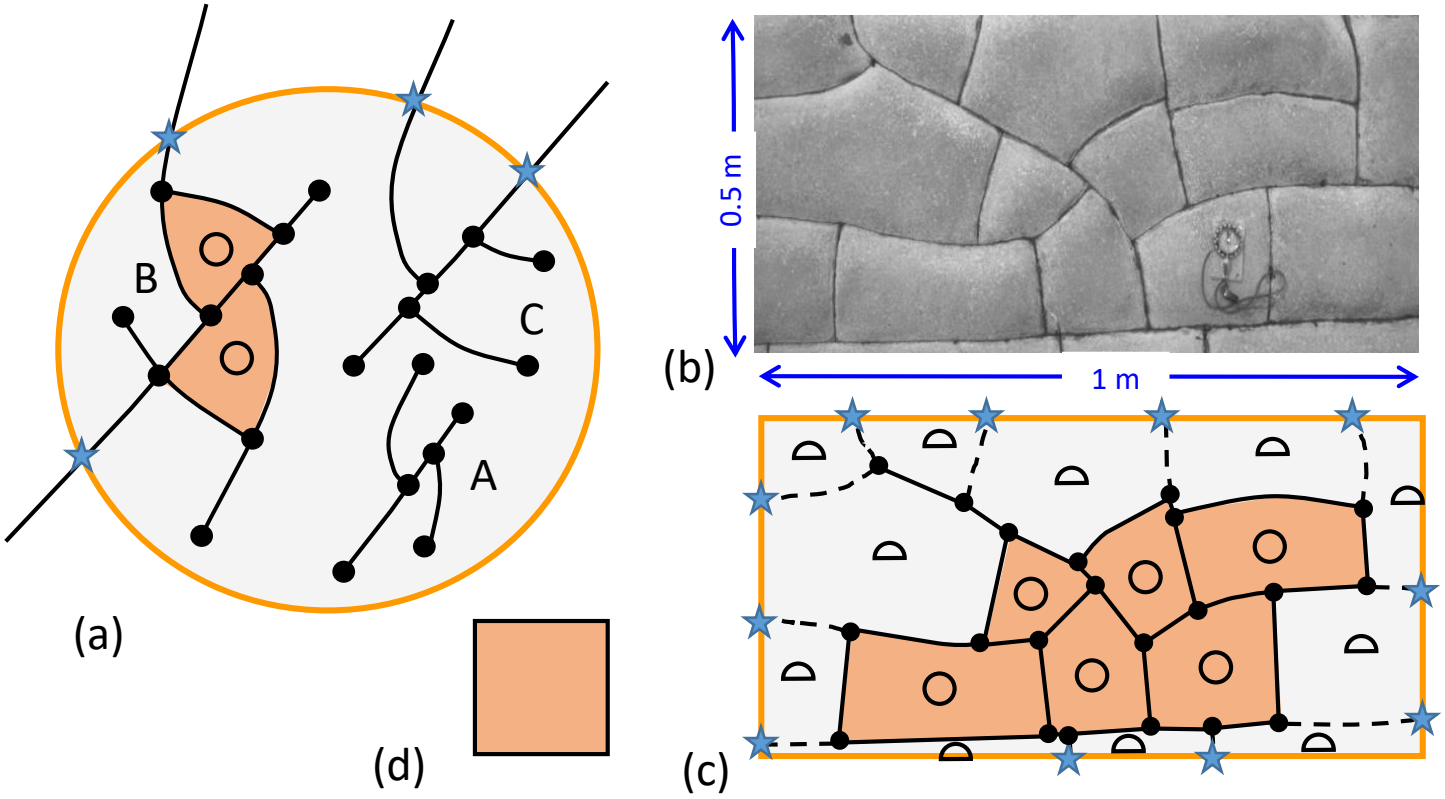

Figure 3

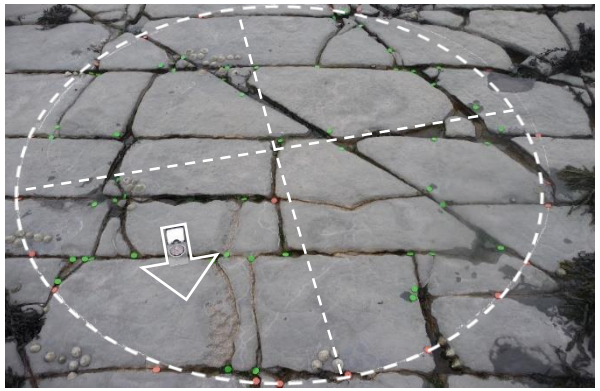

(a)

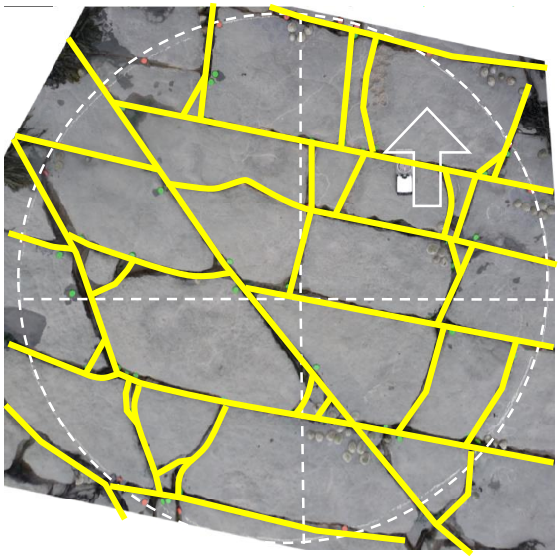

(b)

(c)

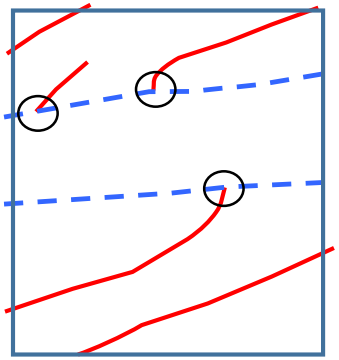

(d)

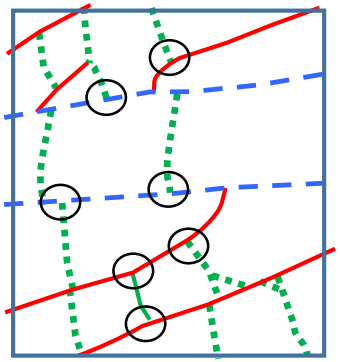

(e)

Figure 4

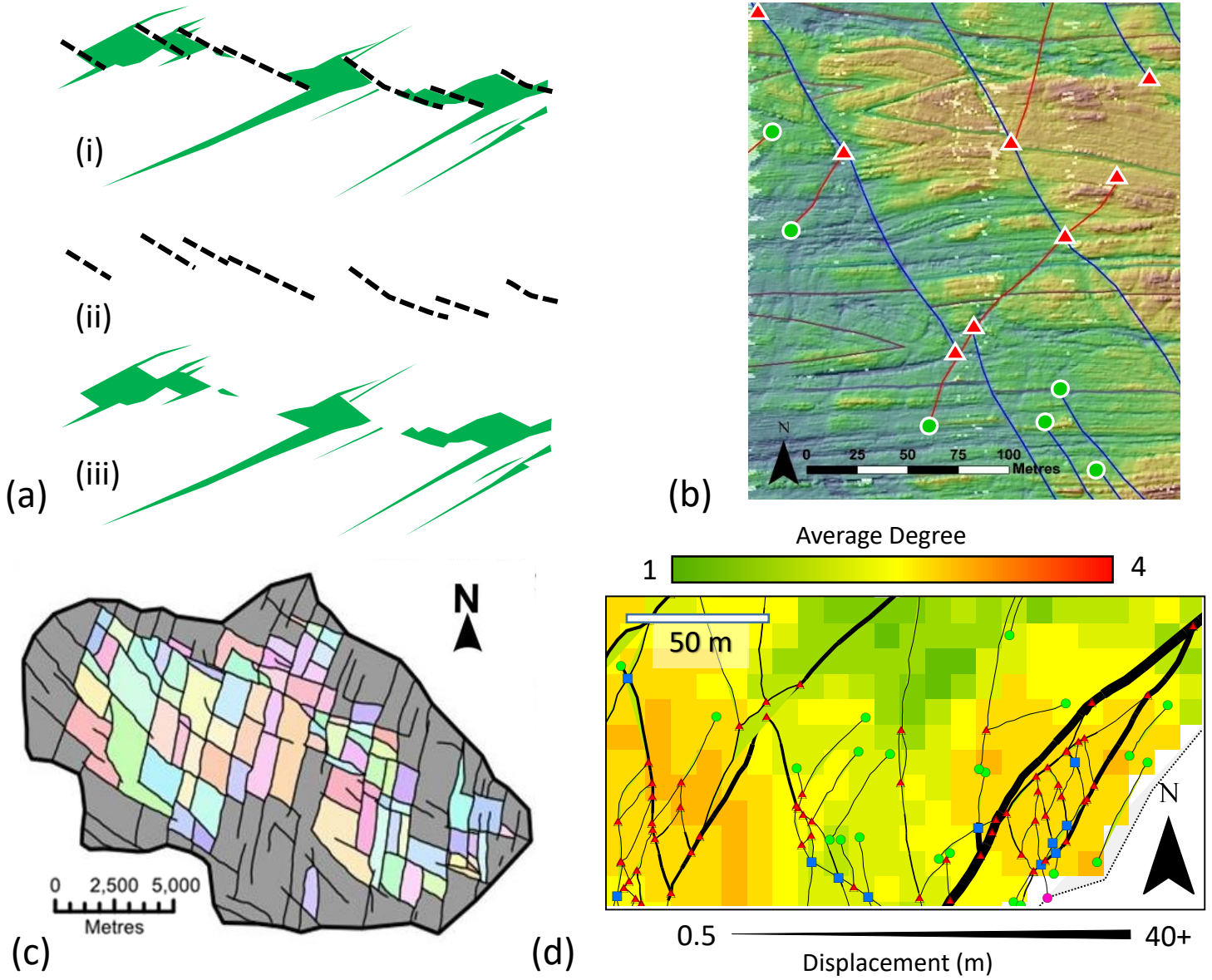
(i)
(ii)
(iii)
(a)
N
0 25 50 75 100
Metres
(b)
N
0 2,500 5,000
Metres
(c)
Average Degree
1
4
50 m
N
0.5
40+
Displacement (m)
(d)

Figure 5

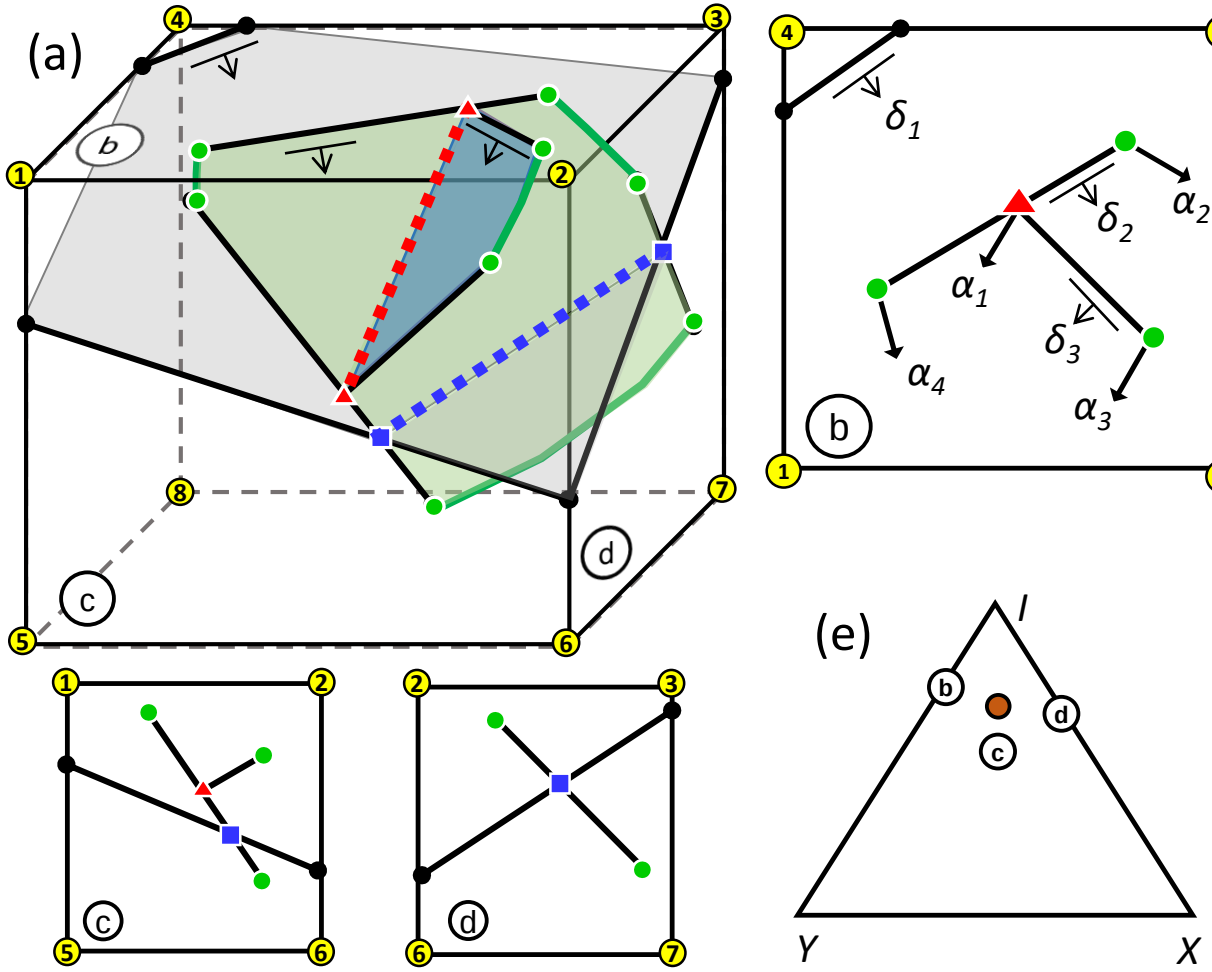
(a)
b
c
d
1
2
3
4
5
6
7
8
δ_1
δ_2
δ_3
α_1
α_2
α_3
α_4
b
(e)
I
Y
X

Figure 6